DOI: 10.1002/chem.200700646

A Theoretical Characterization of the Photoisomerization Channels of 1,2-Cyclononadienes on both Singlet and Triplet Potential-Energy Surfaces

Ming-Der Su*[a]

Abstract: The ground-, $^1(\pi\pi^*)$-, and $^3(\pi\pi^*)$-state potential-energy surfaces of 1,2-cyclononadiene and isomeric C_9H_{14} species, as well as 1-methyl-1,2-cyclononadiene and isomeric $C_{10}H_{16}$ species were all mapped using CASSCF and the 6–31G(d) basis set. Theoretical results were found to be in good agreement with the available experimental observations for both 1,2-cyclononadiene and 1-methyl-1,2-cyclononadiene isomerization reactions under singlet and triplet direct or sensitized irradiation. Extremely efficient decay occurs from the first singlet excited state to the ground state through at least three different conical intersections (surface crossings). The first of these crossing points is accessed by a one-bond ring closure. From this conical intersection point (CI-A or CI-C), some possible subsequent ground-state reaction paths have been identified: 1) intramolecular C–H bond insertion to form the bicyclic photoproduct and 2) intramolecular C–H bond insertion to form tricyclic photoproducts. An excited state [1,3]-sigmatropic shift leads to the second conical intersection (CI-B or CI-E), which can give a three-bond cyclononyne species. Besides these, in the singlet photochemical reactions of 1-methyl-1,2-cyclononadiene, excited-state, one allenic C–H bond insertion leads to a third conical intersection (CI-D). Possible ground-state reaction pathways from this structure lead to the formation of a diene photoproduct or to transannular insertion photoproducts. Moreover, in the case of triplet 1,2-cyclononadiene and 1-methyl-1,2-cyclononadiene photoisomerization reactions, both chemical reactions will adopt a 1,3-biradical (T_1/S_0-1, T_1/S_0-2, and T_1/S_0-3), which may undergo intersystem crossings leading to the formation of tricyclic or bicyclic photoproducts. The results obtained allow a number of predictions to be made.

Keywords: ab initio calculations · cyclononadienes · photochemistry · potential-energy surface

Introduction

The photochemistry and photophysics of olefins has benefited from detailed study, and important information on photochemical processes in general has resulted from these investigations. In contrast, allene photochemistry[1,2] has drawn relatively little attention, and their photochemical reactivity has remained largely unclear. This is particularly true in the case of strained cyclic allenes (cyclic cumulenes). Our knowledge of their photochemical mechanisms remains in a relatively primitive state.[3]

Cyclic cumulene undergoes a rich variety of fundamental photoreactions. The photochemistry of 1,2-cyclononadiene (**1**) was first described in a classic paper by Ward and Karafiath.[4] They reported that the benzene-sensitized photolysis of **1** gave a primary product, tricyclo[4.3.0.0^{2,9}]nonane (**3**, $\varphi = 0.17$ in the vapor phase), and three unidentified photoproducts. Later, through the elegant studies performed by Johnson and many co-workers,[5–10] it was found that the solution- and gas-phase photochemistry of 1,2-cyclononadiene (**1** and **2**) demonstrated a diversity of singlet and triplet excited-state reactions of the allene (1,2-propadiene) chromophore (see Scheme 1). Direct solution phase irradiation of **1** yields tricyclo[4.3.0.0^{2,9}]nonane (**3**), bicyclo[6.1.0]non-1(9)-ene (**4**), and cyclononyne (**5**) as primary photoproducts in a 3:94:3 ratio [Eq. (1) in Scheme 1].[5–7] On the other hand, benzene-sensitized vapor-phase irradiation at 254 nm of **1** yields the previously reported tricyclo[4.3.0.0^{2,9}]nonane (**3**, 89%), in addition to three bicyclics: bicyclo[4.3.0]non-1(2)-ene (**6**, 5%), bicyclo-[4.3.0]non-1(9)-ene (**7**, 4%), and *cis*-bicyclo[4.3.0]non-2-ene (**8**, 2%), as shown in Scheme 1 [Eq. (2)].[5–7] Furthermore,

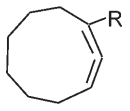

1 R = H
2 R = CH_3

[a] Prof. M.-D. Su
Department of Applied Chemistry
National Chiayi University, Chiayi 60004 (Taiwan)
Fax: (+886) 05-2717901
E-mail: midesu@mail.ncyu.edu.tw

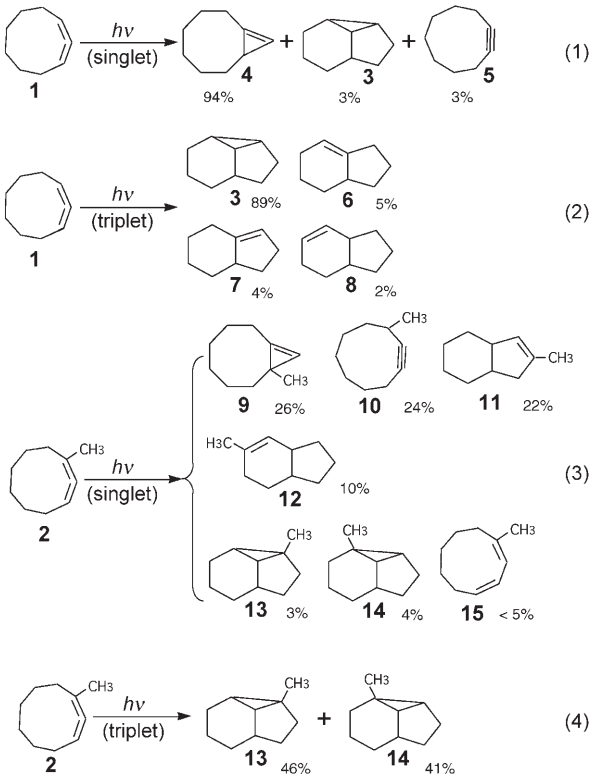

Scheme 1.

the photoreactions of 1-methyl-1,2-cyclononadiene (**2**) were demonstrated and contrasted with those of 1,2-cyclononadiene (**1**).[8] Direct irradiation yields seven isomers as primary products. The major singlet photoproducts are 8-methyl-bicyclo[6.1.0]non-1(9)-ene (**9**, 26%), 3-methyl-cyclononyne (**10**, 24%), *cis*-8-methyl-bicyclo[4.3.0]non-7-ene (**11**, 22%), and *cis*-3-methyl-bicyclo[4.3.0]non-2-ene (**12**, 10%). Minor products from **2** include 2-methyl-tricyclo[4.3.0.$0^{2,9}$]nonane (**13**, 4%), 9-methyl-tricyclo[4.3.0.$0^{2,9}$]nonane (**14**, 3%), and *cic*,*cis*-1-methyl-1,3-cyclononadiene (**15**, $<$ 5%), as given in Scheme 1 [Eq. (3)].[8] Triplet-sensitized reactions of **2** are similar to **1**, affording isomeric tricyclononanes **13** (41%) and **14** (46%) as shown in Scheme 1 [Eq. (4)].[8]

It is these fascinating and seemingly complex experimental results that inspire this study. The key questions are how the various products are formed and why certain products show a significant abundance.[11] A knowledge of the features of the potential-energy hypersurfaces is in general of great value in understanding the roles of the various possible processes. Although these experimental results help in understanding the potential-energy surfaces of excited states in cyclic cumulene systems, they are at present not capable of providing complete mechanistic detail. We were thus curious about exactly how these reactions occur, and wanted detailed mechanistic knowledge, in order to exercise greater control over them. Nevertheless, it is very difficult to detect thermally unstable intermediates and transition structures of ground and excited states, because of their short lifetimes. Theory is therefore a potentially useful partner in the investigation of the mechanism of such photoisomerizations. In particular, to the best of our knowledge, no earlier theoretical work has been performed on the intersections between the different potential surfaces and on the mechanistic aspects of cyclic cumulene photoisomerization reactions.

To understand the reaction mechanisms of the photoreactions of cyclic cumulenes, we undertook an investigation of the potential-energy surfaces of 1,2-cyclononadiene (**1**) and 1-methyl-1,2-cyclononadiene (**2**) in both singlet and triplet states. It is the purpose of this paper to generate the essential parts of the potential surfaces by quantum chemical calculations,[12,13] and to describe the consequences for the reaction mechanisms from such an explicit calculation of the reaction pathways. In the following sections we describe the method and present the results for the photoisomerization reactions of 1,2-cyclononadiene (**1** and **2**) in detail. The intersection points of the ground state (S_0), first excited singlet-state (S_1), and lowest triplet-state (T_1) surfaces and the transition states as well as local minima for isomerizations on S_0, S_1, and T_1 surfaces are determined. Also, the mechanisms, and their implication and comparison with available experiments, are discussed. It will be shown below that the conical intersections[12] and the intersystem crossings play a crucial role in cyclic cumulene singlet and triplet photochemistry.

Computational Methods

All geometries were fully optimized without imposing any symmetry constraints, although in some instances the resulting structures showed various elements of symmetry. The ab initio molecular orbital calculations were performed using the Gaussian 03 software package.[14]

In the investigation of photochemical reaction pathways, the stationary point structures on the S_0, S_1, and T_1 surfaces were optimized at the CASSCF (the complete-active-space SCF) level of calculations using the standard 6–31G(d) basis set.[15] The active space for describing the photoisomerizations of **1** and **2** comprises six electrons in six orbitals, that is, four p-π orbitals plus the σ(C–C) and σ*(C–C) orbitals. In some cases (such as the hydrogen migration reaction), an active space comprising six electrons in six orbitals (π, π, π*, π* in the allenic double bonds and the σ, σ* orbitals in the C–H bond) was used for consistency. Therefore, the active space studied in this work is composed of six electrons in six orbitals, which is referred to as CASSCF(6,6). The state-averaged CASSCF-(6,6) method was used to determine the geometry of the intersection space. The optimization of conical intersections was achieved in the (f−2)-dimensional intersection space using the method of Bearpark et al.[16] implemented in the Gaussian 03 program.

Every stationary point was characterized by its harmonic frequencies computed analytically at the CASSCF level. The harmonic vibrational frequencies of all stationary points were computed analytically to characterize them as minima (all frequencies are real) or transition states (only one imaginary frequency). The optimization was determined when the maximum force and its root mean square (RMS) were less than 0.00045 and 0.00005 hartree bohr^{-1}, respectively. Also, the reactions that we investigated [i.e., the paths in Scheme 1, Eqs. (1–4)] were probed in some detail by determining the intrinsic reaction coordinate (IRC) with the algorithm proposed by Schlegel.[17] In any event, our IRC calculations show that the transition states we found in this work should be true transition states, since they correctly link either the reactants or the critical points. Localization of the minima, transition states, and crossing minima

was performed in Cartesian coordinates; therefore, the results are independent of any specific choice of internal variables. All calculations were carried out on the IBM computers at the National Center for High Performance Computing, with the Gaussian 03 programs.[14]

General considerations: Even though the 1,2-cyclononadiene photoisomerization reported experimentally[5–10] shows a wide variance in its reaction types, it is possible to construct a certain consistency in these reactions, which at least serves as a basis for discussion. In this section, we describe possible excited-state reaction paths that lead to either conical intersections or intersystem crossings. A schematic representation of the relationships between the intersections and possible reaction routes are shown in Schemes 2–5.

As seen in Scheme 1, for the singlet photochemistry of 1,2-cyclononadiene [Eq. (1)],[5–7] the most reasonable pathway for the conversion of **1** to **3**, **4**, and for the conversion of **2** to **9**, **13**, **14**, is the ring closure of the cyclic allene to a cyclopropylidene intermediate (**16**) followed either by hydrogen migration or by insertion into a C–H bond (see Scheme 2).

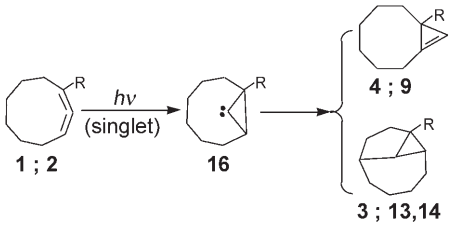

Scheme 2.

Cyclononyne is observed as a singlet photoproduct of both **1** and **2**,[5–8] which implies mechanistic commonality. Hence, a sigmatropic shift mechanism,[1,3] which is based on the Hückel theory (four-electron, photochemically allowed),[18] is proposed for the conversion of 1,2-cyclononadiene (**1** and **2**) to cyclononyne (**5** and **10**, respectively), as illustrated in Scheme 3.

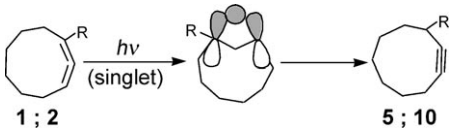

Scheme 3.

Moreover, when one examines the singlet photochemical reactions of **2** [Eq. (3), Scheme 1], 3-methylcyclonon-2-enylidene (**17**) would be proposed as a potential intermediate, from which two transannular insertion products (**11** and **12**) and one diene compound (**15**) are formed.[5–7] This cyclovinylcarbene (**17**) may arise from an excited-state 1,2-shift of the allenyl hydrogen (see Scheme 4).

On the other hand, the cycloallene **1** displays a general type of reaction upon triplet benzene sensitization, i.e., photoisomerization to **3**, **6**, **7**, and **8** [Scheme 1, Eq. (2)] in the vapor phase.[8] This experimental fact strongly implies the existence of a 1,3-biradical species (**18**), and subsequent intersystem crossing to the singlet ground-state products. At this point, three-ring closure or 1,2-hydrogen migration provide straightforward routes to **3** or **6**+**7**+**8** (see Scheme 5).

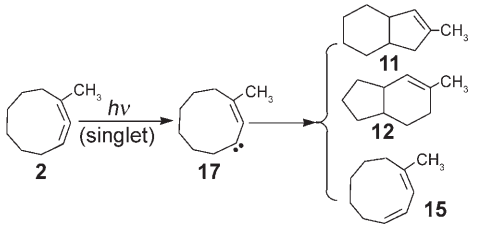

Scheme 4.

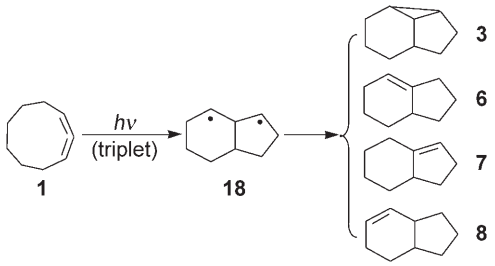

Scheme 5.

Basically, the triplet photoreactions of cycloallene **2** [Eq. (4), Scheme 1] do not differ significantly from those of **1**.[8] In consequence, the biradical mechanism, via an intermediate similar to **18**, can be utilized to explain the observed tricyclononane products (**13** and **14**).

Bearing the above mechanisms (Schemes 2–5) in mind, we located the "funnel" from the excited-state surface to the ground-state surface that corresponds to a conical intersection (or an intersystem crossing) in the following section.

Results and Discussion

Singlet reaction mechanisms of 1,2-cyclononadiene: Let us first consider the photoisomerizations of 1,2-cyclononadiene (**1**). As mentioned previously (see Schemes 2 and 3), two minimum energy pathways on the singlet excited potential-energy surface of **1** were characterized by optimizing the geometries along the $C_1 \cdots C_3$ coordinate (path A) and the $C_1 \cdots H$ coordinate (path B), which lead to photoproducts **3**, **4**, and **5**, respectively. For an understanding of the difference found between these two reaction paths, it is best to start the discussion with the reaction profiles as summarized in Figure 1, which also contains the relative energies of the crucial points with respect to the ground-state minimum **1**. Selected optimized geometrical parameters for the stationary points and conical intersections are collected in Figures 1 and 2, and their corresponding energies are given in Table 1.

In the first step, reactant **1** is promoted to its excited singlet state by a vertical excitation as shown in the middle of Figure 1. After the vertical excitation process, the molecule is situated on the excited-singlet surface, but still possesses the S_0 geometry. According to previous experimental work,[5–7] the photoexcitation of **1** with ≥ 185 nm ($=155$ kcal mol^{-1} in energy) light can lead to the lowest $^1(\pi \rightarrow \pi^*)$ state.[5–7] Our CASSCF result suggests that the calculated $^1(\pi \rightarrow \pi^*)$ excited-state energy at the Franck–Condon geometry (**FC-1**) is 155 kcal mol^{-1}, which is in excellent agreement with the experimental observations.[5–7]

From the point reached by the vertical excitation (**FC-1**) the molecule relaxes to reach an S_1/S_0 conical intersection at which the photoexcited system decays nonradiatively to S_0.[19] The photochemically active relaxation path starting

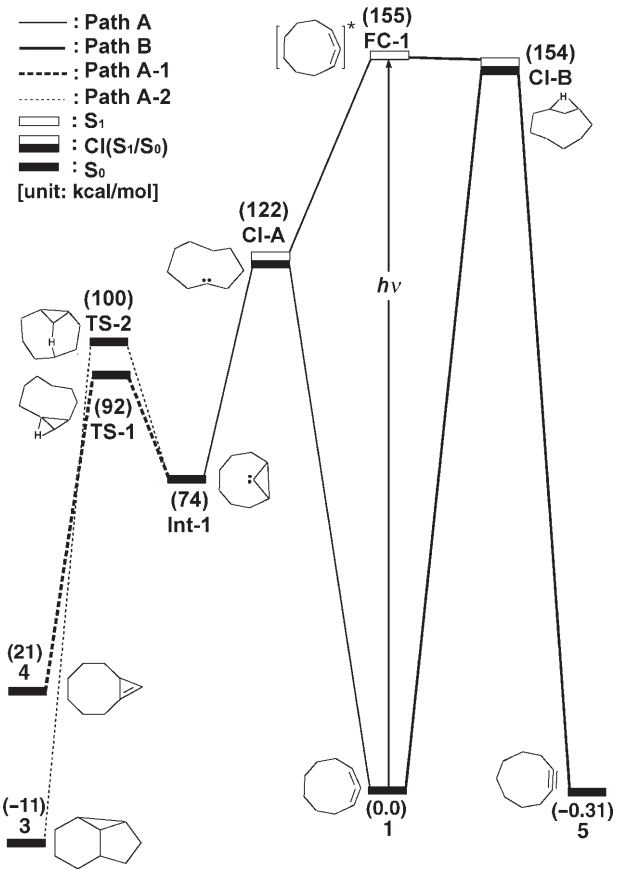

Figure 1. Energy profiles for the singlet photoisomerization modes of 1,2-cyclononadiene (**1**). The abbreviations FC and CI stand for Franck-Condon and conical intersection, respectively. The relative energies were obtained at the CASSCF(6,6)/6–31G(d) level of theory. All energies (in kcal mol^{-1}) are given with respect to the reactant (**1**). For the CASSCF optimized structures of the crucial points see Figures 2 and 3. For more information see the text.

Table 1. Energies along the singlet isomerization reaction pathways (path A and path B) at the CASSCF(6,6)/6–31G(d) levels.[a]

Structure	State	E_{rel} [kcal mol^{-1}] CASSCF(6,6)/6–31G(d)
1	S_0	0.0
FC-1	$^1(\pi\pi^*)$	155.0
CI-A[b]	$^1(\pi\pi^*)$	122.0
	S_0	122.0
Int-1	S_0	73.80
TS-1	S_0	92.28
TS-2	S_0	100.4
3	S_0	−10.62
4	S_0	21.25
CI-B[b]	$^1(\pi\pi^*)$	154.0
	S_0	154.0
5	S_0	−0.3015

[a] Energies relative to 1,2-cyclononadiene (**1**). [b] S_1/S_0 conical intersection.

from the S_1 $^1(\pi\rightarrow\pi^*)$ excited state of **1** leads to the S_1/S_0 **CI-A** and **CI-B**, which are shown on the right-hand (path A) and left-hand (path B) sides of Figure 1, respectively. Both **CI-A** and **CI-B** structures optimized at the CASSCF/6–31G(d) level are shown in Figure 2. The derivative coupling and gradient difference vectors obtained at the conical intersections are also given in Figure 2.

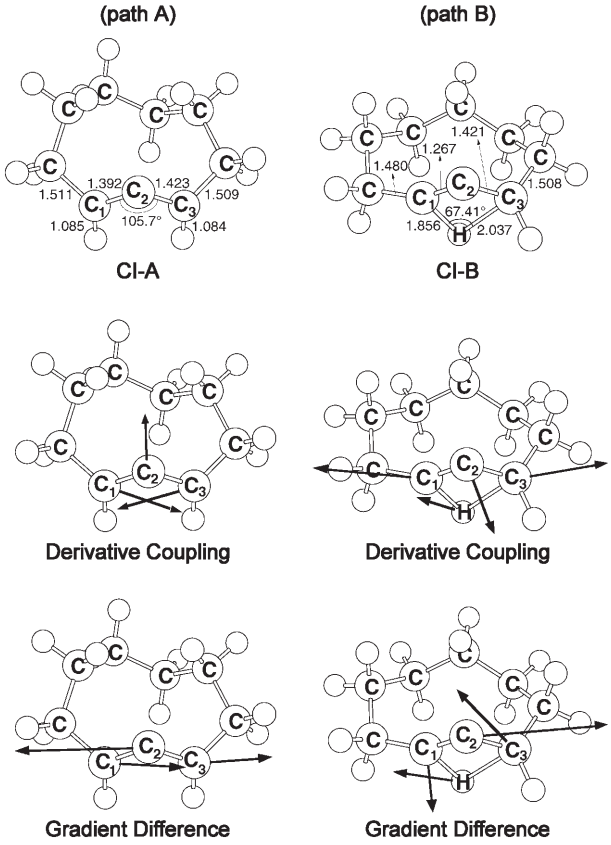

Figure 2. The CASSCF(6,6)/6–31G(d) geometries (bond lengths in Å and angles in °) for the conical intersections (**CI-A** and **CI-B**) of 1,2-cyclononadiene (**1**). The derivative coupling and gradient difference vectors—those which lift the degeneracy—are computed with CASSCF at the conical intersections. The corresponding CASSCF vectors are shown in the inset. For more information see the Supporting Information.

We shall first discuss the S_1/S_0 conical intersection **CI-A**. From Scheme 2, one may foresee that a carbene-like species, cyclopropylidene (**16**), should play a key role in the photorearrangement reactions of **1**. Indeed, along the $C_1C_2C_3$ bending reaction path, a conical intersection, S_1/S_0 **CI-A**, is obtained at the $\measuredangle C_1C_2C_3$ bond angle of 106°. Its optimized structure is given on the left-hand side of Figure 2 with several key structural parameters. Our computational results predict that the energy of **CI-A** lies 122 kcal mol^{-1} above **1** and 33 kcal mol^{-1} below **FC-1**. According to the results demonstrated in Figure 2, examination of these two vectors in **CI-A** provides important information concerning the photoisomerization process of **1**: the derivative coupling vector is mainly related to the $C_1C_2C_3$ bending mode that gives the cyclopropylidene intermediate (**Int-1**) on the S_0 surface, whereas the gradient difference vector gives the asymmetric $C_1C_2C_3$ bending motion that leads to a vibrationally hot **1**-S_0

species. Namely, the cyclopropylidene intermediate (**Int-1**) arises from a singlet excited-state 1,3-closure of the allenyl carbons. The calculated geometry of **Int-1** is shown in Figure 3. Here, as predicted previously (see **16** in Scheme 2), there exists a nonplanar bicyclic structure with a carbene center at the C_2 atom (see Figure 3 for the numbering of the various centers). Moreover, the CASSCF results estimate that the energy of **Int-1** lies below that of **FC-1** by about 81 kcal mol^{-1}. This finding implies that the large excess energy of 81 kcal mol^{-1} resulting from the relaxation from **FC-1** to **Int-1** would be the driving force for further isomerization reactions on the ground-state surface (vide infra).

Then, from **Int-1** isomerization can take place in two directions: one involving hydrogen-atom transfer to the carbene atom (i.e., C_2 in Figure 3) leading to the formation of **4** through a transition state **TS-1** (path A-1), and the other involving a carbene atom undergoing C–H bond insertion to produce **3** via the transition state **TS-2** (path A-2). The optimized transition state structures (**TS-1** and **TS-2**) along with the calculated transition vectors are shown in Figure 3. The heavy arrows in this figure indicate the directions in which the atoms move in the normal coordinate corresponding to the imaginary frequency. Examination of the single imaginary frequency for each transition state (984i cm^{-1} for **TS-1** and 1010i cm^{-1} for **TS-2**) provides excellent confirmation of the above reaction processes.[20] For instance, the reaction vector in **TS-1** is in accordance with the migration process, primarily the C_1–H bond stretching with a hydrogen shifting to the carbene center and a double bond forming between two carbon atoms (i.e., C_1 and C_2). On the other hand, as seen in **TS-2**, the vibrational motion for the insertion of the carbene atom into the intramolecular C_4–H bond involves bond formation between C_2 and C_4 atoms in concert with C_4–H bond breaking and hydrogen transfer to the carbene center. The computational results depicted in Figure 3 reveal that path A-1 and path A-2 can lead to the bicyclic (**4**) and tricyclic (**3**) photoproducts, respectively. As a result, our theoretical investigations suggest that the reaction mechanisms for paths A-1 and A-2 should proceed as shown in Equations (5) and (6), respectively.

$$\mathbf{1}(\mathbf{S_0}) + h\nu \rightarrow \mathbf{FC\text{-}1} \rightarrow \mathbf{CI\text{-}A} \rightarrow \mathbf{Int\text{-}1} \rightarrow \mathbf{TS\text{-}1} \rightarrow \mathbf{4} \quad (5)$$

$$\mathbf{1}(\mathbf{S_0}) + h\nu \rightarrow \mathbf{FC\text{-}1} \rightarrow \mathbf{CI\text{-}A} \rightarrow \mathbf{Int\text{-}1} \rightarrow \mathbf{TS\text{-}2} \rightarrow \mathbf{3} \quad (6)$$

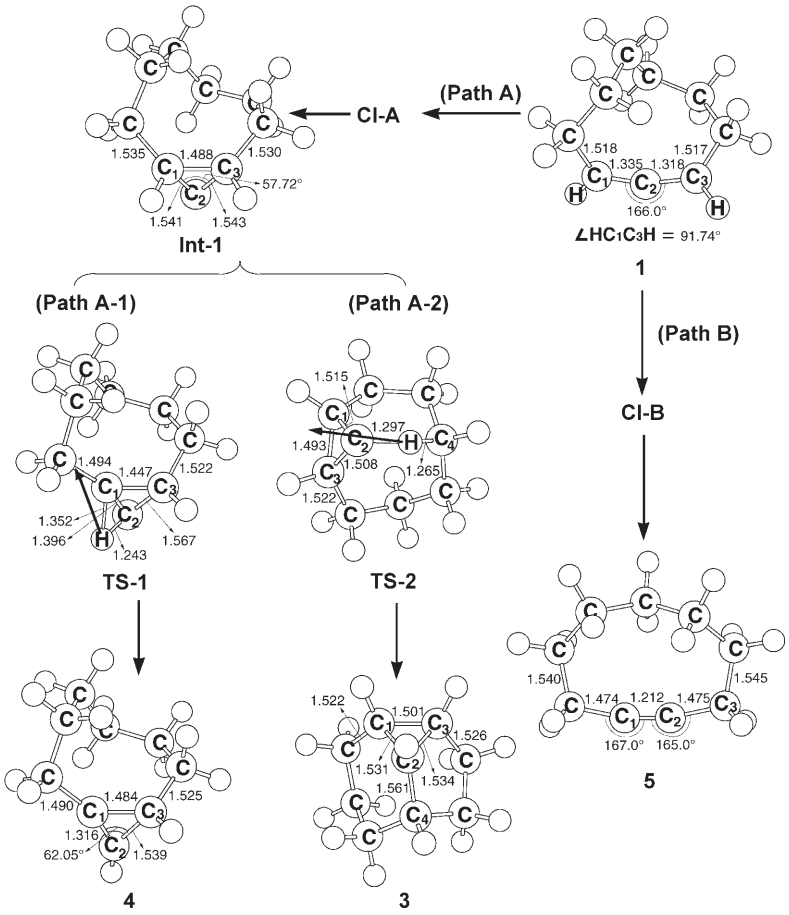

Figure 3. The CASSCF(6,6)/6–31G(d) geometries (bonds lengths in Å and angles °) for the 1,2-cyclononadiene (**1**), conical intersection (**CI-B**), intermediate (**Int-1**), transition states (**TS-1** and **TS-2**), and isomer photoproducts (**3**, **4**, and **5**). The corresponding CASSCF vectors are shown in the inset. For more information see the Supporting Information.

From the local minimum (**Int-1**), the isomerizations possess barrier heights computed to be about 18 kcal mol^{-1} for path A-1 and 26 kcal mol^{-1} for path A-2. That is, one can readily see that the barrier to path A-1 is smaller than that for path A-2. This finding suggests that path A-1 should be more favorable than path A-2 from a kinetic viewpoint. That is to say, it is easier for the photoisomerization of compound **1** to occur through the 1,2-H shift path rather than through C–H bond insertion. These theoretical results are in good agreement with experimental observations that the path A-1 photoproduct (**4**) is in a larger quantum yield than the path A-2 photoproduct (**3**) as demonstrated in Scheme 1.[5–7]

On the other hand, based on Scheme 3, the [1,3] sigmatropic shift mechanism has been proposed to account for the exclusive formation of cyclononyne (**5**) on direct photolysis of **1**. According to this concept, the search for a conical crossing point between S_0 and S_1 surfaces was performed by scanning

both the $\measuredangle C_1C_2C_3$ bending angle and the C_1–H bond length. The relaxation reaches a conical intersection (i.e., S_1/S_0 **CI-B**) where the photoexcited system decays nonradiatively to S_0. As one can see on the right-hand side of Figure 2, the optimized structure of S_1/S_0 **CI-B** has a bicyclic structure with $\measuredangle C_1C_2C_3$ and $\measuredangle C_1HC_3$ bond angles equal to 107 and 67.4°, respectively. Moreover, its C_1–H and C_3–H bond lengths are large (1.86 and 2.04 Å, respectively), compared with regular C–H bond lengths (1.09 Å). Besides these, the derivative coupling vector for S_1/S_0 **CI-B** corresponds to a [1,3] hydrogen migration, while the gradient difference vector corresponds to a concurrent change in the C_1–H and C_2–C_3 bond lengths. The former allows the formation of cycloalkyne (**5**) on the S_0 potential-energy surface, whereas the latter becomes vibrationally hot at the **1**-S_0 configuration. As seen in Figure 1 and Table 1, the CASSCF results suggest that **CI-B** is lower than **FC-1** by only 1.0 kcal mol^{-1} in energy. Accordingly, our computations predict that the photochemical rearrangement reaction of path B should be a barrierless process; that is, starting from the **FC-1** point, 1,2-cyclononadiene (**1**) enters an efficient decay channel, **CI-B**. After decay at this conical intersection point, the triply-bonded photoproduct **5**, as well as the initial reactant **1**, can be reached via a barrierless ground-state relaxation pathway. Thus, our theoretical calculations demonstrate that photoreaction path B of reactant **1** can be represented as **1**(S_0)$+h\nu\rightarrow$**FC-1**$\rightarrow$**CI-B**$\rightarrow$**5**. It should be pointed out that this singlet cycloalkyne formation reaction would be essentially concerted, since decay via the S_1/S_0 (**CI-B**) conical intersection will occur within one vibrational period.[21]

Furthermore, as discussed earlier, our CASSCF results indicate that the relative energies of **CI-A** and **CI-B** with respect to the ground-state minimum **1** are 122 and 154 kcal mol^{-1}, respectively. Consequently, our computational results indicate that path A is not only an energetically but also a dynamically favored electronic relaxation channel for the singlet photoisomerization of **1** to occur from the S_1 surface going through the S_1/S_0 **CI-A** and eventually forming both bicyclic (**4**) and tricyclic (**3**) photoproducts. It is thus anticipated that the quantum yields of the photoproducts of path A should be larger than those of path B. Besides this, due to the lower barrier height for path A-1 than path A-2, it is anticipated that irradiation of **1** should afford predominantly the cyclopropene **4**. These predictions, based on the model calculations presented in this work, are in good accordance with the known experimental observations as mentioned in Equation (1) of Scheme 1.[5–7] Moreover, this theoretical investigation also suggests that the other photochemical funnel (**CI-B**) may be more accessible along the C–H stretching coordinate when sufficient internal energy is provided upon excitation to a hot S_1 state or higher electronic excited states; that is, our computational results indicate that photoreaction path B should give a higher quantum yield of cyclononyne (**5**) when this channel is open upon excitations with sufficient energy. As there are no relevant experimental and theoretical data on such systems, the above result is as yet just a prediction.

Singlet reaction mechanisms of 1-methyl-1,2-cyclononadiene: For comparison, we next consider the photoisomerizations [Eq. (3) in Scheme 1] of 1-methyl-1,2-cyclononadiene (**2**). In this section we shall examine the photochemical reaction pathways corresponding to: 1) a three-membered-ring carbene-like mechanism (Scheme 2), 2) a sigmatropic shift mechanism[1,3] (Scheme 3), and 3) a 1,2-allenyl-hydrogen migration mechanism (Scheme 4). The discussion of these three reaction pathways will be based on 18 fully optimized structures corresponding to minima, transition states, and real crossing points on the S_0 and S_1 ($\pi\pi^*$)-state energy surfaces. A schematic overview of the computed energy profile for the photoreaction pathways of **2** is shown in Figure 4. The structures optimized at the CASSCF/6–31G(d) level are outlined in Figures 5–7, with the corresponding energies given in Table 2.

Table 2. Energies along the singlet isomerization reaction pathways (path C, path D, and path E) at the CASSCF(6,6)/6–31G(d) levels.[a]

Structure	State	E_{rel} [kcal mol^{-1}] CASSCF(6,6)/6–31G(d)
2	S_0	0.0
FC-2	$^1(\pi\pi^*)$	156.1
CI-C[b]	$^1(\pi\pi^*)$	89.82
	S_0	89.82
Int-2	S_0	76.27
TS-3	S_0	83.43
TS-4	S_0	90.71
TS-5	S_0	91.18
9	S_0	31.48
13	S_0	−7.907
14	S_0	−1.161
CI-D[b]	$^1(\pi\pi^*)$	97.33
	S_0	97.33
Int-3	S_0	68.64
TS-6	S_0	80.47
TS-7	S_0	81.70
TS-8	S_0	86.46
11	S_0	−19.43
12	S_0	−22.20
15	S_0	−9.162
CI-E[b]	$^1(\pi\pi^*)$	98.97
	S_0	98.97
10	S_0	3.765

[a] Energies relative to 1-methyl-1,2-cyclononadiene (**2**). [b] S_1/S_0 conical intersection.

Figure 4 is arranged as Figure 1, its center indicating reactant **2** (S_0) and the point on the singlet excited surface reached by a vertical excitation **FC-2** (S_1 (S_0 geom)). The reaction profiles of the three-ring closure (path C) and of the 1,2-H (path D) and 1,3-H (path E) migrations are depicted to the left- and right-hand side of Figure 4, respectively. The calculated singlet vertical excitation energy (**2**$\rightarrow$**FC-2**) is predicted to be about 156 kcal mol^{-1}. This value is in good agreement with experimental work,[8] in which irradiation of dilute pentane solutions of purified **2** with wavelength >185 nm ($=155$ kcal mol^{-1} in energy) lead to the lowest singlet excited state. It should be mentioned that the vertical excitation energy of **1** was also computed to be about

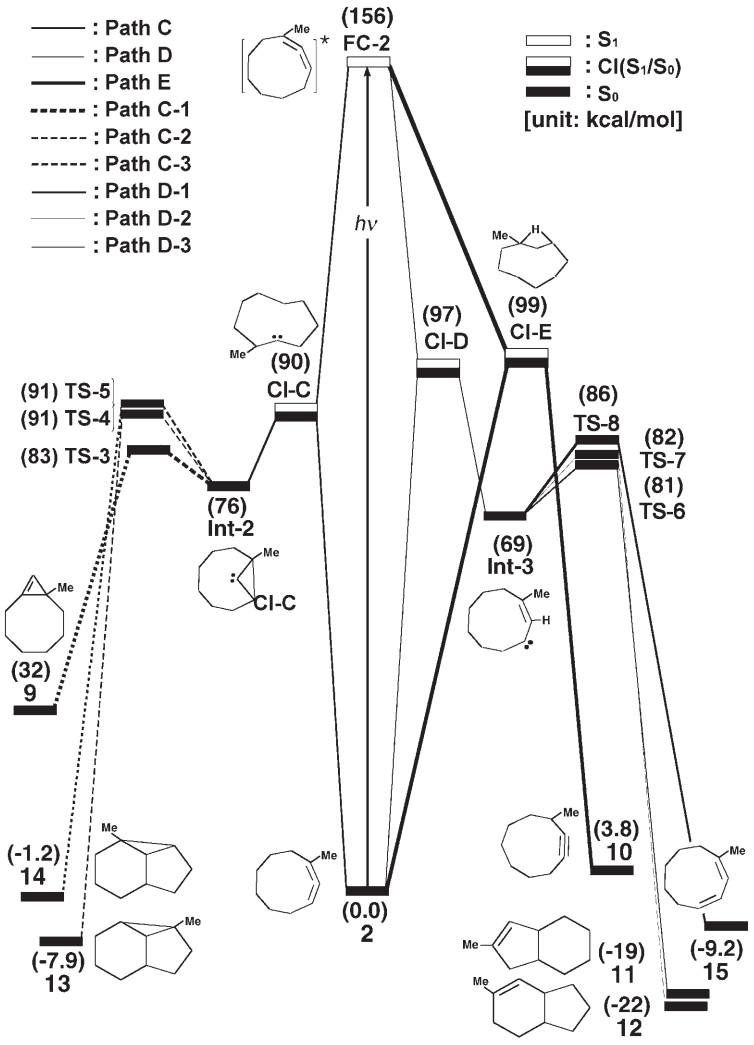

Figure 4. Energy profiles for the singlet photoisomerization modes of 1-methyl-1,2-cyclononadiene (**2**). The abbreviations FC and CI stand for Franck–Condon and conical intersection, respectively. The relative energies were obtained at the CASSCF(6,6)/6–31G(d) level of theory. All energies (in kcal mol^{-1}) are given with respect to reactant **2**. The CASSCF optimized structures of the crucial points see Figures 5–7. For more information see the text.

155 kcal mol^{-1}, as demonstrated in the previous section. From these results, it thus seems that the methyl substituent on the cyclic allene system does not significantly affect the first singlet excitation energy.

The geometry optimization starting from **FC-2** leads to three conical intersections (**CI-C**, **CI-D**, and **CI-E**), which belong to three kinds of reaction pathways, that is, paths C, D, and E, respectively. Their fully optimized structures are collected in Figure 5. The derivative coupling and gradient difference vectors obtained at the conical intersections are also shown in Figure 5.

In path C, as in the case of path A in **1**, geometry optimization on the S_1 $^1(\pi\rightarrow\pi^*)$ excited state was performed by bending the allenic structure of **2**. The relaxation reaches S_1/S_0 **CI-C** where the photoexcited system decays nonradiatively to S_0. As seen in Figure 5, the two allenyl C–C bond lengths (C_1–C_2 and C_2–C_3) are greater than average, 1.411 Å, and the allenyl angle ($\measuredangle C_1C_2C_3$) is narrowed to 107.3°. For comparison, the corresponding allenyl C–C bond lengths are 1.327 Å and the allenyl angle is 165.7° at the ground-state minimum **2**. As a result, the nature of the relaxation of **2** on the path C potential-energy surface can be regarded as C_1–C_3 bond closure. Besides this, according to the results outlined in Figure 5, funneling through S_1/S_0 **CI-C** leads to two different reaction paths on the ground-state surface, through either the derivative coupling vector or the gradient difference vector.[12] The derivative coupling vector for **CI-C** corresponds to an antisymmetric bending motion, which may lead to a vibrationally hot species at the S_0 configuration. On the other hand, its gradient difference vector corresponds to the intramolecular formation of a three-membered ring species. Indeed, following the gradient difference vector from **CI-C** and decreasing the $\measuredangle C_1C_2C_3$ bond angle, the system arrives at a bicyclic intermediate with a carbene center, **Int-2**. It should be emphasized that the geometrical structure of **Int-2** is consistent with the previously proposed mechanism shown in Scheme 2, in which bicyclic intermediate **16** itself bears the three-membered ring carbene character. Moreover, this carbene species is expected to have a short lifetime before ring closure to the bicyclic and tricyclic photoproducts occurs. Many different options are available to the molecule once it is in this intermediate state. With regard to the structure of **Int-2**, the search for transition states on the S_0 surface gives **TS-3**, **TS-4**, and **TS-5** for reaction paths C-1, C-2, and C-3, respectively (Figure 6).[20] For instance, for path C-1, hydrogen migration to a bicyclic photoproduct, 8-methyl-bicyclo[6.1.0]non-1(9)-ene (**9**), will occur through a unimolecular 1,2-hydrogen shift (**TS-3**). Thus, the process of path C-1 can be described as given in Equation (7).

$$\mathbf{2}(\mathbf{S_0}) + h\nu \rightarrow \mathbf{FC\text{-}2} \rightarrow \mathbf{CI\text{-}C} \rightarrow \mathbf{Int\text{-}2} \rightarrow \mathbf{TS\text{-}3} \rightarrow \mathbf{9} \qquad (7)$$

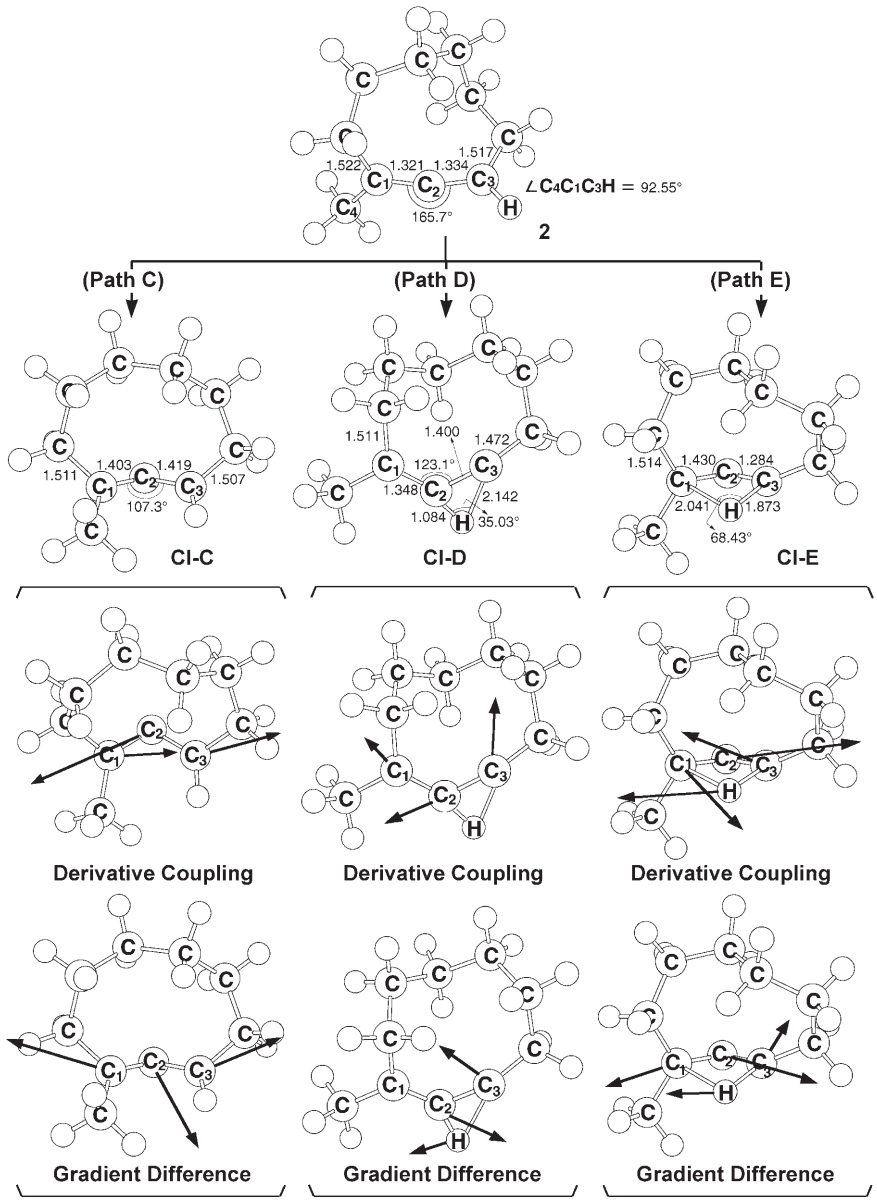

Figure 5. The CASSCF(6,6)/6–31G(d) geometries (bond lengths in Å and angles in °) for the conical intersections (**CI-C**, **CI-D**, and **CI-E**) of 1-methyl-1,2-cyclononadiene (**2**). The derivative coupling and gradient difference vectors—those which lift the degeneracy—are computed with CASSCF at the conical intersections. The corresponding CASSCF vectors are shown in the inset. For more information see the Supporting Information.

Alternatively, the formation of isomeric tricyclic products could occur. The ring closure isomerization leads to methyl-substituted strained tricyclics (**13** and **14**) by way of an intramolecular 1,2-hydrogen migration between two carbon atoms, accompanied by C–C bond formation (**TS-4** and **TS-5**, respectively). Accordingly, our theoretical investigations suggest that paths C-2 and C-3 can proceed as shown in Equations (8) and (9), respectively.

$$\mathbf{2}(\mathbf{S_0}) + h\nu \rightarrow \mathbf{FC\text{-}2} \rightarrow \mathbf{CI\text{-}C} \rightarrow \mathbf{Int\text{-}2} \rightarrow \mathbf{TS\text{-}4} \rightarrow \mathbf{13} \quad (8)$$

$$\mathbf{2}(\mathbf{S_0}) + h\nu \rightarrow \mathbf{FC\text{-}2} \rightarrow \mathbf{CI\text{-}C} \rightarrow \mathbf{Int\text{-}2} \rightarrow \mathbf{TS\text{-}5} \rightarrow \mathbf{14} \quad (9)$$

As can be seen in Figure 4 and Table 2, the theoretical results suggest that **CI-C** is 66 kcal mol^{-1} lower in energy than **FC-2**, but 90 kcal mol^{-1} higher in energy than the ground-state reactant **2**. Additionally, the **Int-2** intermediate was calculated to be thermodynamically less stable than reactant **2** by 76 kcal mol^{-1}, but more stable than **CI-C** by 14 kcal mol^{-1}. Further, our CASSCF calculations demonstrate that the isomerization barriers for paths C-1, C-2, and C-3 are about 7.0, 15, and 15 kcal mol^{-1} higher in energy, respectively, than the intermediate **Int-2**. Accordingly, due to the high excess energy of 66 kcal mol^{-1} resulting from the relaxation from **FC-2** to **CI-C**, the barrier heights of **TS-3**, **TS-4**, and **TS-5** can easily be overcome. Moreover, our theoretical investigations predict that reaction path C-1 should be more favorable than paths C-2 and C-3 from a kinetic viewpoint. This prediction was confirmed by the available experimental results.[8] As already shown in Equation (3) (Scheme 1), it was experimentally reported that the quantum yield of bicyclic photoproduct **9** (26%) is much larger than those of isomeric tricyclic photoproducts **13** (3%) and **14** (4%).

In path D, as discussed in Scheme 4, 3-methylcyclonon-2-enylidene (**17**) was considered as a potential intermediate in singlet photoreactions of **2** [Eq. (2)]. To investigate this, geometry optimization on the S_1 excited state was performed from the 1,2-allenyl-hydrogen migration structure of **2**. In the present study, this conical intersection (**CI-D**) has been fully optimized and located at the $\measuredangle C_2HC_3$ bond angle of 35.03°, and with the two C–H bond lengths equal to 1.084 and 2.142 Å, respectively. Its key structural parameters are given in Figure 5, accompanied by the derivative coupling vector and the gradient difference vector. The derivative coupling vector and the gradient difference vector in **CI-D** correspond to changes in the C_1–C_2 and C_2–C_3 bond lengths and the C_1–C_2 and C_3–H bond lengths, respectively. An in-

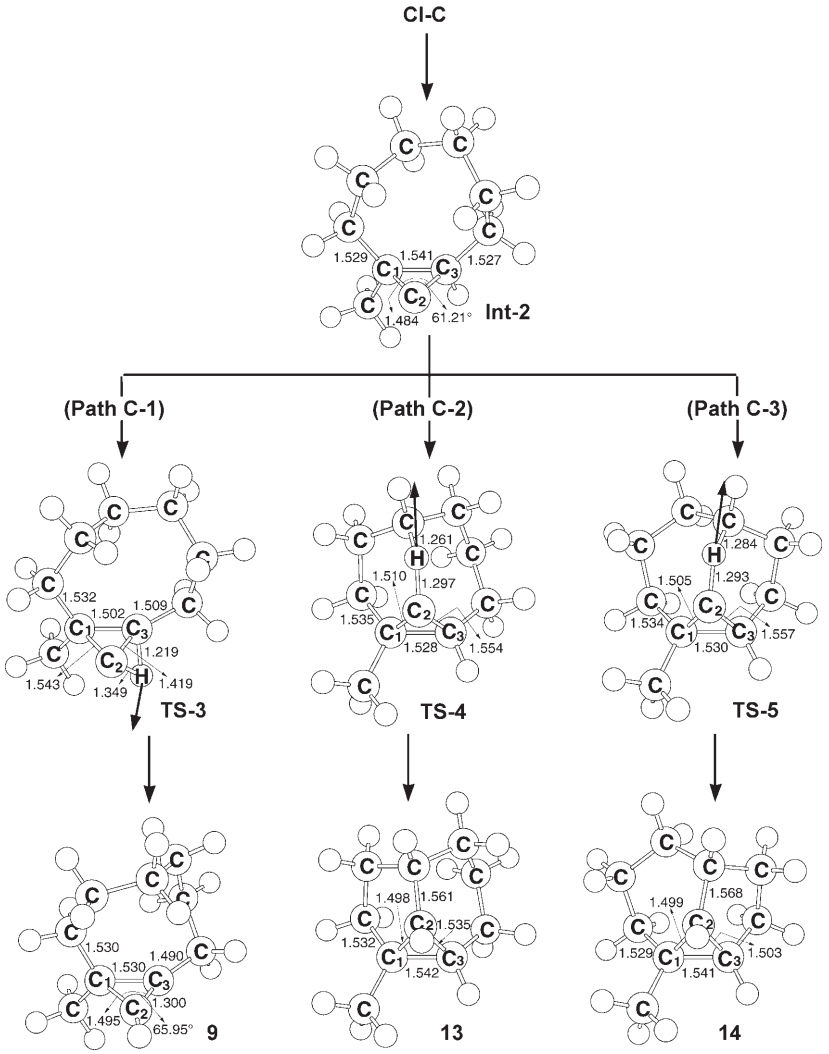

Figure 6. The CASSCF(6,6)/6–31G(d) geometries (bond lengths in Å and angles in °) for pathway C of 1-methyl-1,2-cyclononadiene (**2**). They include intermediate (**Int-2**), transition states (**TS-3**, **TS-4**, and **TS-5**), and isomer photoproducts (**9**, **13**, and **14**). The corresponding CASSCF vectors are shown in the inset. For more information see the Supporting Information.

crease in the C_3–H bond length coupled with a decrease in the C_1–C_2 bond length leads to a local minimum, **Int-3**. Indeed, such 1,2-H migration (C_3 to C_2) and C_1-C_2-C_3 bending motions can result in the *syn*-vinylcarbene conformation **Int-3**. It should be emphasized that this [1,2]-sigmatropic shift species is in accordance with the previous proposed intermediate (**17**) shown in Scheme 4.

Basically, the reaction profile computed for path D resembles that of path C, as shown on the right- and left-hand sides of Figure 2, respectively. Namely, starting from the carbene intermediate **Int-3**, isomerization reactions on the ground state energy surface can take three different directions: the intramolecular C–H bond insertion in **Int-3** to produce bicyclic alkenes **11** and **12** (paths D-1 and D-2, respectively), and a 1,2-H shift leading to the formation of the monocyclic diene **15** (path D-3). The main geometrical parameters of the transition states corresponding to these rearrangement reactions are collected in Figure 7, together with the meaningful components of their transition vectors. These transition states will be referred to as **TS-6**, **TS-7**, and **TS-8** for paths D-1, D-2, and D-3, respectively. Regarding the intramolecular C–H bond insertion, one can observe that the main components of the transition vector correspond to the motion of the hydrogen atom between the two carbon atoms (paths D-1 and D-2). The computed eigenvalues give imaginary frequencies of 948i cm^{-1} (**TS-6**) and 966i cm^{-1} (**TS-7**).[20] Indeed, inspection of the transition vector shows clearly that the reaction proceeds toward the formation of bicyclic alkenes (**11** and **12**, respectively). On the other hand, the transition state located for the 1,2-H migration of path D-3 is characterized by one imaginary frequency of 1332i cm^{-1} for **TS-8**. The normal coordinate corresponding to the imaginary frequency is primarily located at the C–H bond cleavage. Again, taken together these features indicate that the rearrangement reactions proceed as given in Equations (10–12).

$$\mathbf{2}(S_0) + h\nu \rightarrow \textbf{FC-2} \rightarrow \textbf{CI-D} \rightarrow \textbf{Int-3} \rightarrow \textbf{TS-6} \rightarrow \mathbf{11} \quad (10)$$

$$\mathbf{2}(S_0) + h\nu \rightarrow \textbf{FC-2} \rightarrow \textbf{CI-D} \rightarrow \textbf{Int-3} \rightarrow \textbf{TS-7} \rightarrow \mathbf{12} \quad (11)$$

$$\mathbf{2}(S_0) + h\nu \rightarrow \textbf{FC-2} \rightarrow \textbf{CI-D} \rightarrow \textbf{Int-3} \rightarrow \textbf{TS-8} \rightarrow \mathbf{15} \quad (12)$$

As seen in Figure 4 and Table 2, our CASSCF calculations indicate that the energy of **CI-D** relative to the ground-state minimum (**2**) is 97 kcal mol^{-1}, and lower than **FC-2** by 59 kcal mol^{-1}. The carbene intermediate, **Int-3**, was located 69 kcal mol^{-1} higher than **2**. From this local minimum, the three rearrangement reactions possess small barriers, computed to be about 12 kcal mol^{-1} for path D-1 (**Int-3**→**TS-6**), 13 kcal mol^{-1} for path D-2 (**Int-3**→**TS-7**), and 17 kcal mol^{-1} for path D-3 (**Int-3**→**TS-7**). Owing to the large excess energy (59 kcal mol^{-1}) produced by decay from **FC-2** to

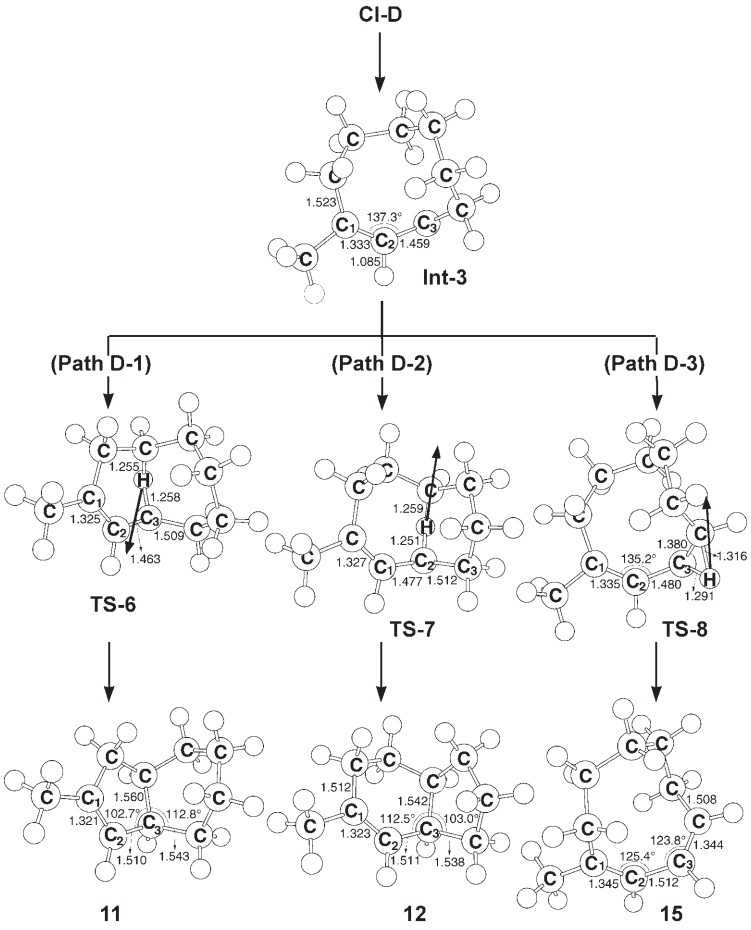

Figure 7. The CASSCF(6,6)/6–31G(d) geometries (bond lengths in Å and angles in °) for pathway D of 1-methyl-1,2-cyclononadiene (**2**). They include intermediate (**Int-3**), transition states (**TS-6**, **TS-7**, and **TS-8**), and isomer photoproducts (**11**, **12**, and **15**). The corresponding CASSCF vectors are shown in the inset. For more information see the Supporting Information.

Int-3, it is expected that this relaxation energy is sufficient to provoke the effective photoisomerization reactions (paths D-1, D-2, and D-3) for **2** (vide infra).

Finally, as already proposed in Scheme 3, one attractive possibility for the **2**→**10** (3-methyl-cyclononyne) conversion is a concerted four-electron mechanism (photochemically allowed).[19] This requires 1,3-hydrogen migration and simultaneous 1,2-carbon bonding. In fact, as a cycloalkyne is observed as a singlet photoproduct of both **1** and **2**, this implies mechanistic commonality. As a result, the production of the cycloalkyne via the S_1/S_0 surface intersection discussed for **1** can serve as a model for reactant **2** investigated here. In path E, the local point of the potential-energy surface is the conical intersection, **CI-E**. Geometrical parameters and relative energies for **CI-E** are given in Figure 5 and Table 2, with the numbering of atoms shown previously, in which H is the migrating hydrogen atom. The derivative coupling and gradient difference vectors obtained at this conical intersection are also shown in Figure 5. From the **CI-E** structure in Figure 5, it is evident that the migrating hydrogen atom, which is in a nearly planar allenic environment, interacts with the two terminal allenic carbons. Consequently, the characteristic of the **CI-E** structure (and the **CI-B** structure) is common to the H/allyl conical intersections reported as ubiquitous control elements in photochemical sigmatropic shifts.[21] Following the gradient difference vector from **CI-E** (Figure 5) and decreasing the C_1–H distance leads to the formation of cyclononyne (**10**). As seen in Figure 4 and Table 2, **CI-E** is located 99 kcal mol^{-1} above the ground-state minimum (**2**), and 57 kcal mol^{-1} below **FC-2**, while photoproduct **10** is less stable than reactant **2** by 3.8 kcal mol^{-1}. Our theoretical observations therefore suggest that the monocylic alkyne (**10**) is the product of an extremely efficient decay channel along a [1,3]-sigamatropic shift reaction pathway via a conical intersection. As mentioned earlier, such a 1,3-H migration in **2** would lead to a real conical intersection (S_1/S_0 **CI-E**), at which the decay to the ground-state surface occurs within a single vibrational period[21] and thus follows a concerted pathway.[22]

In principle, the photoreaction mechanisms of 1-methyl-1,2-cyclononadiene (**2**) are described as above and contrasted with those of 1,2-cyclononadiene (**1**). Direct irradiation yields as primary products seven isomers as demonstrated in Equation (3) (Scheme 1). The major singlet product is best accounted for by excitation-state 1,3-carbon closure to a cyclopropylidene intermediate (i.e., **CI-C**→**Int-2**). This singlet photoreaction has the lowest energy conical intersection (90 kcal mol^{-1}), as well as the lowest kinetic barrier (8.0 kcal mol^{-1}) as discussed above, which is in excellent agreement with the known experimental result.[8] The quantum yields of other minor photoproducts decrease in the order: **10** (24%) > **11** (22%) > **12** (10%) > **14** (4%) > **13** (3%) > **15** (<5%).[8] These experimental observations can be best accounted for by our CASSCF study as demonstrated in Figure 4.

Triplet reaction mechanisms of 1,2-cyclononadiene: Let us now turn to the triplet photoisomerization reactions of **1** [Eq. (2) in Scheme 1]. Figure 8 displays the relative energies on the triplet potential-energy surface along the assumed photoisomerization pathways from **1** to various photoproducts (**3**, **6**, **7**, and **8**). Selected optimized geometrical parame-

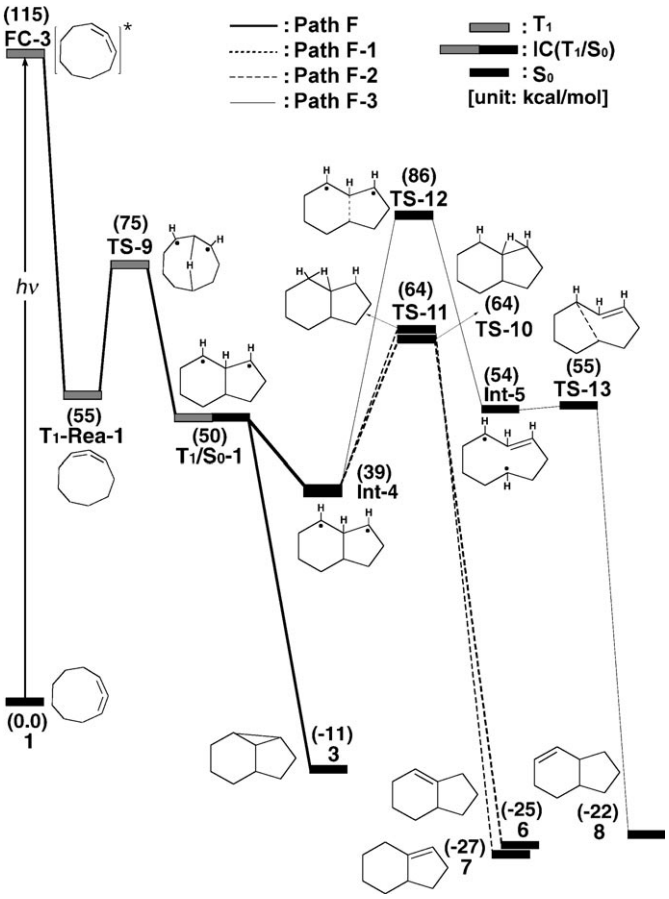

Figure 8. Energy profiles for the triplet photoisomerization modes of 1,2-cyclononadiene (**1**). The abbreviation FC stands for Franck–Condon. The relative energies were obtained at the CASSCF(6,6)/6–31G(d) level of theory. All energies (in kcal mol^{-1}) are given with respect to the reactant (**1**). For the CASSCF optimized structures of the crucial points see Figures 9 and 10. For more information see the text.

ters for the critical points of Equation (2) and their energies on the ground- and lowest triplet-state surfaces can be taken from Figures 9 and 10 and Table 3.

In the first step the reactant **1** is excited to its lowest lying triplet state (T_1) by a vertical excitation. After the vertical excitation process the molecule is situated on the triplet surface, but still possesses the ground-state (S_0) geometry. This point on the triplet surface is denoted as **FC-3** (T_1 (S_0 geom)). In fact, the calculated vertical excitation energy can be taken as an indication of overall accuracy. The computed triplet vertical excitation energy of compound **1** is 115 kcal mol^{-1} ($S_0 \rightarrow T_1$ (S_0 geom)). Comparison with the corresponding experimental value of 254 nm[7,9] (=113 kcal mol^{-1} in energy) for the T_1 state indicates that the present calculations can provide a good estimate of the relative energies for cyclic allene systems.

From the Franck-Condon point **FC-3**, the molecule may relax to a local minimum near to the S_0 geometry. This local minimum of the triplet surface is denoted **T_1-Rea-1**, which is calculated to be about 55 kcal mol^{-1} above the ground-state minimum, as illustrated in Figure 8. The optimized geometrical parameters of **T_1-Rea-1** are given in Figure 9. Comparing the **T_1-Rea-1** geometry (Figure 9) with that of its corresponding ground-state minimum **1** (Figure 3), it is readily seen that the triplet state has significantly larger bond lengths (C_1–C_2 and C_2–C_3) but a narrower bond angle ($\measuredangle C_1C_2C_3$) than its closed shell singlet state. The reason for this phenomenon can be understood simply by considering their electronic structures.[23] Molecular orbital theory[23] predicts that the triplet state of an allene adopts a planar structure, while its singlet ground state possesses a perpendicular one. Our CASSCF results confirm this prediction. For instance, the ground-state minimum **1** adopts an antiplanar structure with a $\measuredangle HC_1C_3H$ dihedral angle of 91.74° (Figure 3). The rotation of one methylene through about 90° gives the nearly planar form ($\measuredangle HC_1C_3H = 1.270°$) of the first excited triplet **T_1-Rea-1** (Figure 9).

Table 3. Energies along the triplet isomerization reaction pathway (path F) at the CASSCF(6,6)/6–31G(d) levels.[a]

Structure	State	E_{rel} [kcal mol^{-1}] CASSCF(6,6)/6–31G(d)
1	S_0	0.0
FC-3	$^3(\pi\pi^*)$	114.6
T_1-Rea-1	$^3(\pi\pi^*)$	54.59
TS-9	$^3(\pi\pi^*)$	75.21
T_1/S_0-1	$^3(\pi\pi^*)$	50.09
3	S_0	−10.62
Int-4(triplet)	$^3(\pi\pi^*)$	39.14
Int-4(singlet)	S_0	39.14
TS-10	S_0	64.03
TS-11	S_0	64.06
TS-12	S_0	86.48
Int-5	S_0	54.05
TS-13	S_0	54.87
6	S_0	−25.21
7	S_0	−26.89
8	S_0	−22.15

[a] Energies relative to 1,2-cyclononadiene (**1**) at the ground state.

Then, from the local minimum **T_1-Rea-1**, a transition state search for the hydrogen migration based on the model of the **T_1-Rea-1** conformation was undertaken. As seen in **T_1-Rea-1** in Figure 9, one hydrogen atom (H′) is significantly closer to the allene center carbon (C_2), its distance being 2.749 Å. We ascribe the regioselective ring hydrogen migration to this skewed structure. In fact, this conformation is necessary for the transannular insertion that leads to **3**, **7**, **6**, and **8**, the observed final photoproducts. The computational results predict that **TS-9** on the $^3(\pi\pi^*)$ surface (Figure 8 and Table 3) is located at an energy 40 kcal mol^{-1} below the vertical excitation energy (**FC-3**), but about 20 kcal mol^{-1} higher in energy than **T_1-Rea-1**, where we started the search. The nature of this saddle point was analyzed by computations of the vibrational frequencies. The optimized transition state structure (**TS-9**) along with the calculated transition vector at the CASSCF level is shown in Figure 9. The arrows indicate the direction in which the atoms move in the normal coordinate corresponding to the imaginary frequency (2980i cm^{-1}).[20] That is, the vibrational motion for the intramolecular insertion of a carbene into the C_4–H′

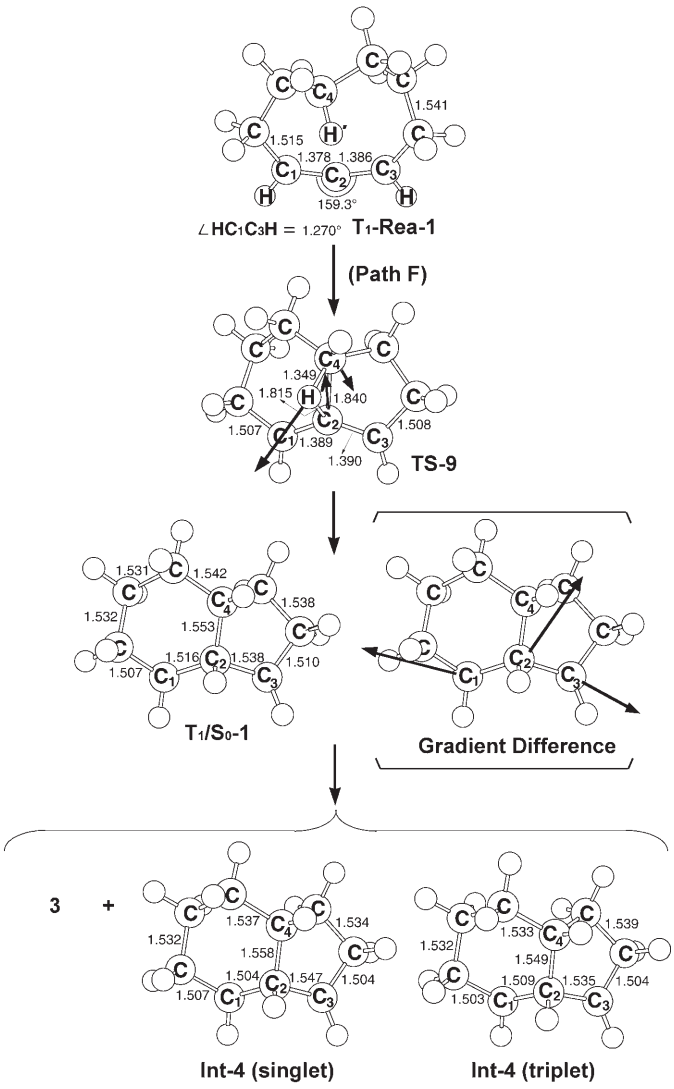

Figure 9. The CASSCF(6,6)/6–31G(d) geometries (bond lengths in Å and angles in °) for pathway F of 1,2-cyclononadiene (**1**). They include the first triplet reactant (**T_1-Rea-1**), transition state (**TS-9**), intersection crossing (**T_1/S_0–1**), and intermediates (**Int-4(singlet)** and **Int-4(triplet)**). The gradient difference vector, which lifts the degeneracy, was computed with CASSCF at the intersection crossing. The corresponding CASSCF vectors are shown in the inset. For more information see the Supporting Information.

bond involves the formation of a C_2–C_4 bond and a C_2–H′ bond.

According to the experimental observations,[7] it has been found that the photoisomerization of **1** (Eq. (2)) is nonadiabatic. The reaction starts from the T_1 surface and proceeds ultimately along the ground-state (S_0) pathway. Thus, the crossing points of the T_1 and S_0 surfaces should play an important role in determining the photorearrangement reactions of Equation (2). Intersystem crossing from the $^3(\pi\pi^*)$ to the $^1(\pi\pi^*)$ state takes place in the region of the T_1/S_0 intersection **T_1/S_0-1**, as illustrated in Figure 8. The structure of **T_1/S_0-1**, as given in Figure 9, was determined using the state-averaged CASSCF(6,6) method with the 6–31G(d) basis set. Basically, **T_1/S_0-1** is a bicyclic species with C_1–C_2 and C_2–C_3 almost equal bond lengths (1.527 Å). The corresponding relative energy of the crossing point **T_1/S_0-1** is shown in Table 3 and Figure 8. Our theoretical investigation indicates that the **T_1/S_0-1** point is located 65 kcal mol^{-1} below the **FC-3** point, and 50 kcal mol^{-1} above the ground-state minimum, **2**. The gradient difference vector of **T_1/S_0-1** given in Figure 9, through the **T_1/S_0-1** point, indicates that the system can access either a tricyclic photoproduct **3** or a biradical intermediate **Int-4** (Figure 9). The molecule at the **Int-4** point has a bicyclic structure with a fusion of five- and six-membered rings. The unpaired electrons lie on the C_1 and C_3 atoms, but these two electrons are far enough apart so that its singlet and triplet states are degenerate (Table 3). The optimized structures (along with selected bond parameters) of the singlet and triplet states of **Int-4** are illustrated in Figure 9. It is apparent that both singlet (**Int-4(singlet)**) and triplet (**Int-4(triplet)**) states are not distinguishable in structure. The calculated energies of the **Int-4(singlet)** and **Int-4(triplet)** structures are given in Table 3, from which one can see that the two points have the same energy (about 39 kcal mol^{-1} above the ground-state minimum **2**). Again, the above results clearly show that the S_0 and T_1 surfaces intersect at the same point. Our theoretical results estimate that **Int-4** lies 16 kcal mol^{-1} below the triplet local minimum **T_1-Rea-1**. Thus, our theoretical observations suggest that the short-lived **Int-4(singlet)** intermediate can be formed from a fast **T_1/S_0-1** crossing followed by a decay through the other **Int-4(triplet)/Int-4(singlet)** intersystem crossing. That is to say, the presence of the two-level degeneracy means that decay to the ground state will be efficient from the lowest triplet-state surface.

Once decay through the bicyclic biradical **Int-4** has occurred, there are three different reaction paths available on the ground-state surface: a 1,2-H shift to produce the bicyclic products, **6** (denoted path F-1) and **7** (denoted path F-2), and a ring open–closure mechanism which results in the formation of a new bicyclic photoproduct **8** (denoted path F-3), can all compete. The optimized geometrical parameters of the related stationary points can be found in Figure 10. As a result, the mechanisms of triplet photoisomerizations of 1,2-cyclononadiene (**1**) are represented in Equations (13)–(16), paths F, F-1, F-2, and F-3, respectively. All these routes are likely to be accessible, as the molecule will have a great deal of excess energy once it has decayed through an intersystem crossing point.

$$\mathbf{1}(\mathbf{S_0}) + h\nu \rightarrow \mathbf{FC\text{-}3} \rightarrow \mathbf{T_1\text{-}Rea\text{-}1} \rightarrow \mathbf{TS\text{-}9} \rightarrow \mathbf{T_1/S_0\text{-}1} \rightarrow \mathbf{3} \tag{13}$$

$$\mathbf{1}(\mathbf{S_0}) + h\nu \rightarrow \mathbf{FC\text{-}3} \rightarrow \mathbf{T_1\text{-}Rea\text{-}1} \rightarrow \mathbf{TS\text{-}9} \rightarrow \mathbf{T_1/S_0\text{-}1} \rightarrow \mathbf{Int\text{-}4} \rightarrow \mathbf{TS\text{-}10} \rightarrow \mathbf{6} \tag{14}$$

$$\mathbf{1}(\mathbf{S_0}) + h\nu \rightarrow \mathbf{FC\text{-}3} \rightarrow \mathbf{T_1\text{-}Rea\text{-}1} \rightarrow \mathbf{TS\text{-}9} \rightarrow \mathbf{T_1/S_0\text{-}1} \rightarrow \mathbf{Int\text{-}4} \rightarrow \mathbf{TS\text{-}11} \rightarrow \mathbf{7} \tag{15}$$

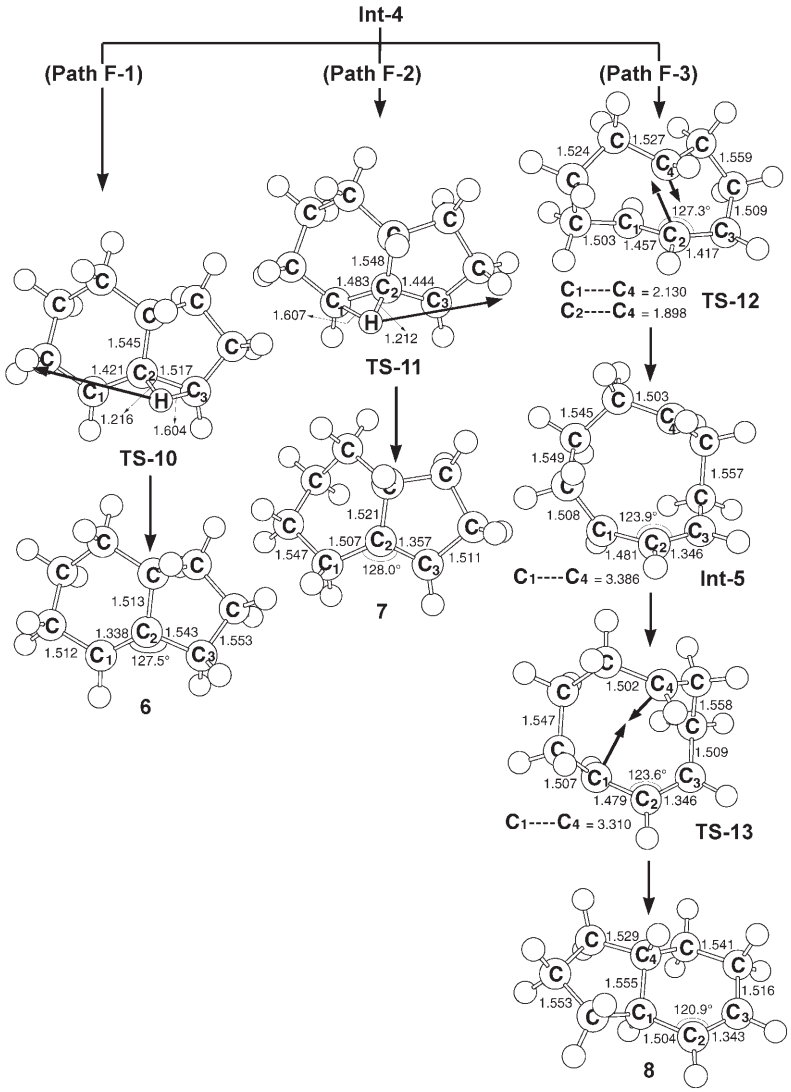

Figure 10. The CASSCF(6,6)/6–31G(d) geometries (bond lengths in Å and angles in °) for pathway F of 1,2-cyclononadiene (**1**). They include transition states (**TS-10**, **TS-11**, **TS-12**, and **TS-13**), intermediate (**Int-5**), and isomer photoproducts (**6**, **7**, and **8**). The corresponding CASSCF vectors are shown in the inset. For more information see the Supporting Information.

$$\mathbf{1}(S_0) + h\nu \rightarrow \mathbf{FC\text{-}3} \rightarrow \mathbf{T_1\text{-}Rea\text{-}1} \rightarrow \mathbf{TS\text{-}9} \rightarrow \mathbf{T_1/S_0\text{-}1} \rightarrow \mathbf{Int\text{-}4} \rightarrow \mathbf{TS\text{-}12} \rightarrow \mathbf{Int\text{-}5} \rightarrow \mathbf{TS\text{-}13} \rightarrow \mathbf{8} \quad (16)$$

It is worth noting that the existence of the **Int-4(triplet)/Int-4(singlet)** intersection leads the $T_1 \rightarrow S_0$ process to occur via the **Int-4** point. The **Int-4** point acts as a relay and enables the T_1 to S_0 intersection crossing to occur with high efficiency, and plays an essential role in the relaxation dynamics of the T_1 state of 1,2-cyclononadiene **1**.

As seen in Figure 8 and Table 3, the activation barrier of **TS-12** (by path F-3) is apparently larger than that of **TS-10** (by path F-1) and **TS-11** (by path F-2). That is, the CASSCF calculations show that **TS-12** (86 kcal mol^{-1}) > **TS-10** ≈ **TS-11** (64 kcal mol^{-1}) with respect to the ground-state minimum **1**. Thus, our theoretical findings strongly suggest that both path F-1 and path F-2 are preferred over path F-3. Accordingly, based on the above computational results, one may then anticipate that, in the triplet photoisomerization of **1**, the tricyclic molecule **3** should be the predominant photoproduct, while the quantum yields of the other bicyclic products decrease in the order **6** ≈ **7** > **8**. Our theoretical findings are in good accordance with the experimental observations as illustrated in Scheme 1.[7,9]

Triplet reaction mechanisms of 1-methyl-1,2-cyclononadiene: Finally, we describe the triplet photorearrangement reactions of 1-methyl-1,2-cyclononadiene [**2**: Eq. (4) in Scheme 1]. Figure 11 displays the relative energies for critical points on the triplet potential-energy surface from **2** to isomeric tricyclononanes (**13** and **14**). Selected geometric values and the relative energies based on CASSCF(6,6)/6–31G(d) calculations for all stationary points and crossing points (intersystem crossing) of **2** at the lowest-lying triplet state are reported in Figure 12 and Table 4, respectively.

As in the case of 1,2-cyclononadiene (**1**), the triplet photorearrangement reactions of **2** studied in this work follow similar reaction paths to those shown earlier. Based on the CASSCF(6,6)/6–31G(d) structure of the ground-state **2**, the vertical excitation energy from S_0 to T_1 ($S_0 \rightarrow T_1$ (S_0 geom)) was calculated to be about 110 kcal mol^{-1} (**FC-4**) above the ground-state reactant **2**. The experimental triplet vertical excitation energy of **2** is 113 kcal mol^{-1} (=254 nm),[8] which agrees well with the present computational result. It is therefore believed that the present model compound with the method employed in this study should provide reliable information for the discussion of the triplet photochemical reaction mechanisms of **2**.

Once the $S_0 \rightarrow T_1$ vertical excitation occurs, the system will relax from the **FC-4** point to the T_1 minimum (**T_1-Rea-2**), the latter being lower in energy by 54 kcal mol^{-1} than the former. The optimized geometrical parameters of **T_1-Rea-2** can be found in Figure 12. By analogy with the case of **1**, the CASSCF results indicate that the lowest-lying triplet state of **2** (**T_1-Rea-2**) has a significantly narrower bond angle

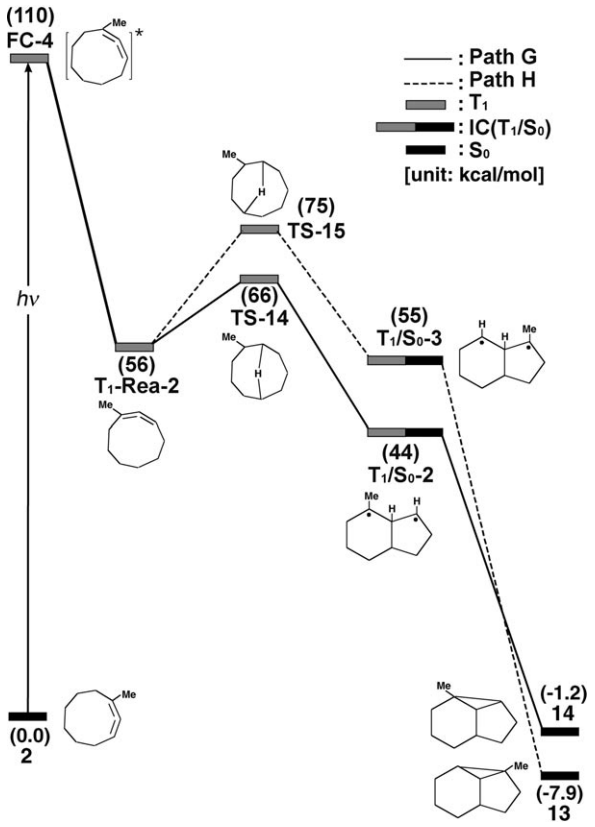

Figure 11. Energy profiles for the triplet photoisomerization modes of 1-methyl-1,2-cyclononadiene (**2**). The abbreviation FC stands for Franck-Condon. The relative energies were obtained at the CASSCF(6,6)/6–31G(d) level of theory. All energies (in kcal mol^{-1}) are given with respect to the reactant (**2**). For the CASSCF optimized structures of the crucial points see Figure 12. For more information see the text.

($\measuredangle C_1C_2C_3 = 159.0°$) and larger bond lengths (i.e., C_1–C_2, C_2–C_3 = 1.387, 1.381 Å, respectively) than its closed shell singlet state equivalent (see Figure 5). Again, the reason for this phenomenon can be understood simply by considering the electronic structures of the two states.[23] It is worth noting that only the antiplanar structure is stable for **2** with a dihedral angle $\measuredangle C_4C_1C_3H$ of 92.55°, whereas the minimum point (**T_1-Rea-2**) corresponding to a planar structure was located for the triplet state of **2**, with a dihedral angle $\measuredangle C_4C_1C_3H$ of 0.6600°, on the CASSCF potential-energy surface. These results are consistent with those reported for **1** in the previous section. To the best of our knowledge, neither experimental nor theoretical work on the triplet substituted 1,2-cyclononadiene has been reported previously.

From **T_1-Rea-2**, isomerization to the final photoproducts (**13** and **14**) can involve two reaction pathways as demonstrated in Figure 11. On the one hand, the system may undergo a transannular insertion between atoms C_2 and C_6 via a transition state **TS-14** (path G). On the other hand, decay may proceed by a transannular insertion between atoms C_2 and C_7 through a transition state **TS-15** (path H). Vibrational frequency calculations show that both **TS-14** and **TS-15** are real transition states with one imaginary frequency on the triplet potential-energy surface. The optimized transition state structures (**TS-14** and **TS-15**) along with the calculated transition vectors are shown in Figure 12. It is apparent that these transition states connect the triplet local minimum **T_1-Rea-2** to the corresponding intersystem crossing points (**T_1/S_0-2** and **T_1/S_0-3**, respectively).[20] The single imaginary frequency for each transition state (1093i cm^{-1} for **TS-14** and 1105i cm^{-1} for **TS-15**) provides a confirmation of an intramolecular insertion process. Our CASSCF calculations suggest that formation of **T_1/S_0-2** from **T_1-Rea-2** proceeds via transition state **TS-14** with a low energy barrier of 10 kcal mol^{-1} (path G), while **T_1/S_0-3** is formed through transition state **TS-15** with an energy barrier of 19 kcal mol^{-1} (path H). In consequence, from the reaction profiles shown in Figure 11, it is evident that this system has sufficient internal energy to overcome the energy barrier between the **T_1-Rea-2** minimum and the **T_1/S_0-2** (or **T_1/S_0-3**) intersection after photoexcitation to the T_1 state (vide infra).

The optimized geometries of **T_1/S_0-2** and **T_1/S_0-3** are illustrated in Figure 12, with the gradient difference vectors. Basically, the structures of the two intersection points involve a fusion of a five- and a six-membered ring, with two unpaired electrons lying on the C_1 and C_3 atoms. It is evident that these two unpaired electrons are far enough apart to result in their singlet and triplet states being degenerate. Consequently, the S_0 and T_1 surfaces can intersect at the same point. Furthermore, as seen in Figure 12, there are large components of stretching on the allenic bonds, implying that ring closure will occur with no barrier. As shown in Table 4 and Figure 11, the relative energies of **T_1/S_0-2** and **T_1/S_0-3** were calculated to be lower than their corresponding triplet transition states by 22 and 20 kcal mol^{-1}, but higher than the singlet ground-state minimum (**2**) by 44 and 55 kcal mol^{-1}, respectively. Accordingly, from an energetic viewpoint, once reactant **2** has populated the T_1 state by photoexcitation, it would relax to the **T_1-Rea-2** minimum with sufficient internal energy to overcome barriers on the T_1 surface to reach one of the **T_1/S_0** intersection points. From here ring closure follows to yield the isomeric tricyclononanes (**13** and **14**). In short, the ring-closure mechanism of triplet photoisomerization of 1-methyl-1,2-cyclononadiene (**2**) can be represented by Equations (17) and (18), paths G and H, respectively.

$$\mathbf{2}(S_0) + h\nu \rightarrow \mathbf{FC\text{-}4} \rightarrow \mathbf{T_1\text{-}Rea\text{-}2} \rightarrow \mathbf{TS\text{-}14} \rightarrow \mathbf{T_1/S_0\text{-}2} \rightarrow \mathbf{14} \quad (17)$$

$$\mathbf{2}(S_0) + h\nu \rightarrow \mathbf{FC\text{-}4} \rightarrow \mathbf{T_1\text{-}Rea\text{-}2} \rightarrow \mathbf{TS\text{-}15} \rightarrow \mathbf{T_1/S_0\text{-}3} \rightarrow \mathbf{1} \quad (18)$$

As discussed above, our computations predict a local minimum to which the molecules relax after the vertical excitation. From this minimum, both transannular insertion modes possess small barriers, so that both routes can be taken. It should be taken into account that the molecules possess an excess energy of 54 kcal mol^{-1} arising from the relaxation to the triplet local minimum. It is therefore anticipated that both path G and path H should compete with each other.

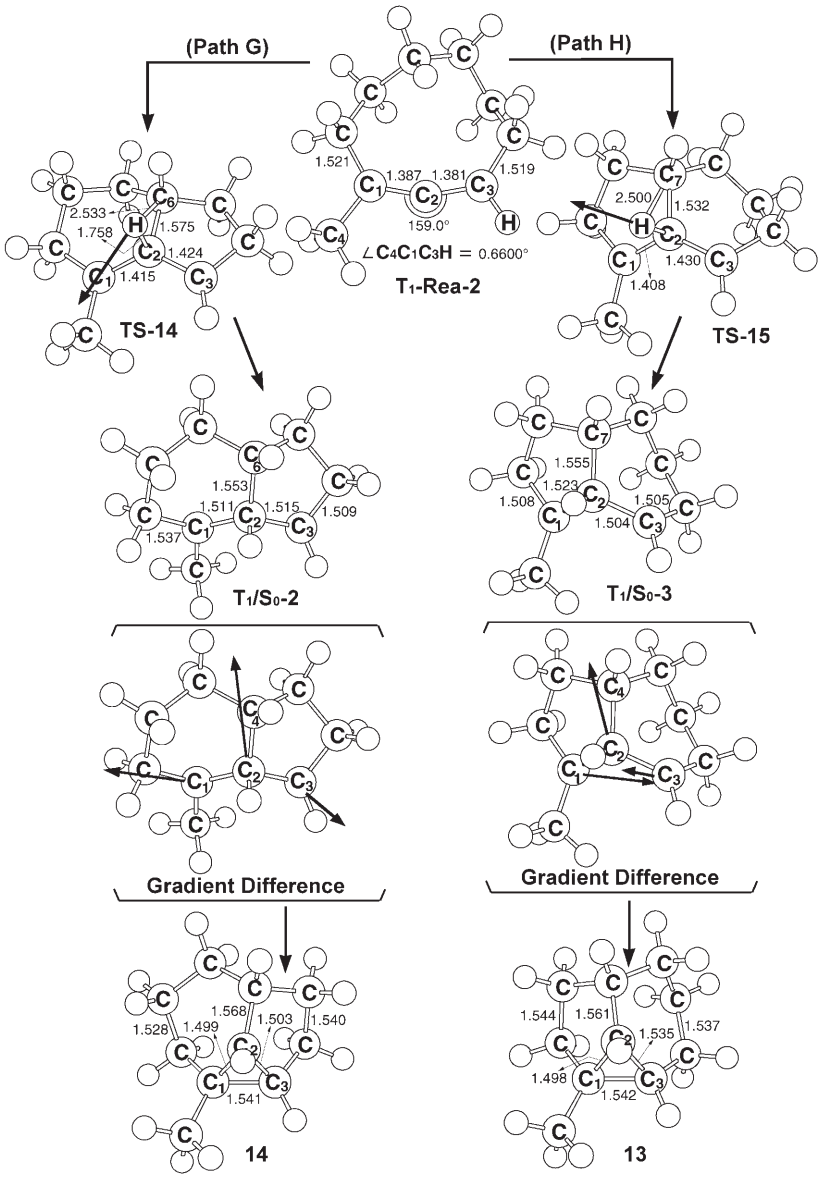

Figure 12. The CASSCF(6,6)/6–31G(d) geometries (bond lengths in Å and angles in °) for pathways G and H of 1-methyl-1,2-cyclononadiene (**2**). They include the first triplet reactant (**T_1-Rea-2**), transition states (**TS-14** and **TS-15**), intersection crossings (**T_1/S_0–2** and **T_1/S_0–3**), and isomer photoproducts (**13** and **14**). The gradient difference vector, which lifts the degeneracy, was computed with CASSCF at the intersection crossing. The corresponding CASSCF vectors are shown in the inset. For more information see the Supporting Information.

This prediction is in good accordance with the available experimental evidence[8] [see Eq. (4) in Scheme 1]. It was experimentally reported that vapor-phase irradiation of **2** with benzene at 254 nm resulted in two predominant products (**13** and **14**) with nearly equal quantum yields.[24]

Conclusions

In this work, we have used ab initio CASSCF calculations to study the mechanisms of the photoisomerizations of 1,2-cyclononadiene and 1-methyl-1,2-cyclononadiene. By exploring the $^1(\pi\pi^*)$ and $^3(\pi\pi^*)$ potential-energy surfaces near the S_0 equilibrium structure and in the regions of several surface crossings, we are able to present a comprehensive and detailed picture of the photochemical processes of 1,2-cyclononadiene and 1-methyl-1,2-cyclononadiene under singlet and triplet direct or sensitized irradiation. On the basis of the energies and structures of the minima, transition states, and crossing points, we can draw the following conclusions:

1) We have identified at least three kinds of regions on the singlet potential-energy surfaces at which the $^1(\pi\pi^*)$ and ground-state surfaces cross. These surface crossings are represented in Scheme 2 (ring closure to form bicyclic carbene), Scheme 3 (a [1,3]-sigmatropic shift), and Scheme 4 (a [1,2]-sigmatropic shift to form monocyclic carbene), respectively. Once decay through the conical intersections has occurred, there are many different reaction paths available on the ground-state surface. Schemes 2–4 and reversion back to 1,2-cyclononadiene or 1-methyl-1,2-cyclononadiene can all compete. In the case of conical intersections (such as CI-A–CI-E), there are also the options of efficient interconversion leading to vibrationally ex-

Table 4. Energies along the triplet isomerization reaction pathways (path G and path H) at the CASSCF(6,6)/6–31G(d) levels.[a]

Structure	State	E_{rel} [kcal mol^{-1}] CASSCF(6,6)/6–31G(d)
2	S_0	0.0
FC-4	$^3(\pi\pi^*)$	110.2
T_1-Rea-2	$^3(\pi\pi^*)$	56.33
TS-14	$^3(\pi\pi^*)$	66.18
TS-15	$^3(\pi\pi^*)$	75.08
T_1/S_0-2	$^3(\pi\pi^*)$	54.61
13	S_0	−7.907
T_1/S_0-3	$^3(\pi\pi^*)$	43.96
14	S_0	−1.161

[a] Energies relative to 1-methyl-1,2-cyclononadiene (**2**) at the ground state.

cited 1,2-cyclononadiene or 1-methyl-1,2-cyclononadiene. All these routes are likely to be accessible, as the molecule will have a great deal of excess energy once it has decayed through a conical intersection.

2) Our study strongly points out that these conical intersections (i.e., CI-A–CI-E, respectively) on the singlet potential-energy surfaces play a crucial role in determining the reaction pathways as well as the quantum yields of the various photoproducts. In particular, it was found that the existence of a low-lying conical intersection provides a highly effective radiationless decay channel.[12,13] For instance, see singlet photoisomerizations of cyclic cumulenes in Figures 1 and 4. The theoretical findings shown in this work are in excellent agreement with many experimental observations that have been reported for these species.
3) We have identified one kind of region on the triplet potential-energy surface where the $^1(\pi\pi^*)$, $^3(\pi\pi^*)$, and ground-state surfaces cross. This intersurface crossing is given in Scheme 5 (formation of a metastable 1,3-biradical which closes to form bicyclic or tricyclic photoproducts). The fast radiationless decay of triplet 1,2-cyclononadiene or 1-methyl-1,2-cyclononadiene to the ground state originates from a narrowing of the T_1/S_0 gap, which results from the relaxation of the T_1 state to a bicyclic structure (1,3-biradical, i.e., **T_1/S_0-1**, **T_1/S_0-2**, and **T_1/S_0-3**, respectively). These facts may account for one main triplet photoproduct (**3**) and several minor triplet photoproducts (**6**–**8**) in the 1,2-cyclononadiene system, representing competitive 1,3-biradical pathways. Triplet-sensitized reactions of **2** are similar to **1**, affording isomeric tricyclononanes (**13** and **14**).

It is hoped that the present work can stimulate further research into this subject.

Acknowledgements

The author is grateful to the National Center for High-Performance Computing of Taiwan for generous amounts of computing time, and the National Science Council of Taiwan for financial support. The author also wishes to thank Professor Michael A. Robb, Dr. Michael J. Bearpark, (University of London, UK), Professor Massimo Olivucci (Universita degli Studi di Siena, Italy), and Professor Fernando Bernardi (University of Bologna, Italy) for their encouragement and support. Special thanks are also due to one referee for very helpful suggestions and comments.

[1] For reviews, see: a) W. D. Huntsman, in *The Chemistry of Ketenes, Allenes, and Related Compounds, Part 2* (Ed.: S. Patai), Wiley, New York, **1980**, pp. 650–657; b) *The Chemistry of the Allenes, Vols. 1–3* (Ed.: S. R. Landor), Academic Press, New York, **1982**; c) M. G. Steinmetz, R. Srinivasan, W. J. Leigh, *Rev. Chem. Intermed.* **1984**, *5*, 57.

[2] a) H. I. Karan, *J. Org. Chem.* **1981**, *46*, 2186; b) C. S. Drucker, V. G. Toscano, R. G. Weiss, *J. Am. Chem. Soc.* **1973**, *95*, 6482; c) O. Rodriquez, H. Morrison, *J. Chem. Soc. D* **1971**, 679; d) H. R. Ward, E. Karafiath, *J. Am. Chem. Soc.* **1969**, *91*, 7475; e) O. L. Chapman, *Pure Appl. Chem.* **1974**, *40*, 511; f) D. C. Lankin, D. M. Chihal, N. S. Bhacca, G. W. Griffin, *J. Am. Chem. Soc.* **1975**, *97*, 7133; g) M. G. Steinmetz, R. T. Mayes, J.-C. Yang, *J. Am. Chem. Soc.* **1982**, *104*, 3518; h) J. C. Berridge, J. Forrester, B. E. Foulger, A. Gilbert, *J. Chem. Soc. Perkin Trans.* **1980**, 2425; i) K. Fujita, K. Matsui, T. Shono, *J. Am. Chem. Soc.* **1975**, *97*, 6256; j) M. W. Klett, R. P. Johnson, *Tetrahedron Lett.* **1983**, *24*, 1107.

[3] For reviews, see: a) R. P. Johnson, *Org. Photochem.* **1985**, *7*, 75; b) R. P. Johnson in *Molecular Structure and Energetics, Vol. 3* (Eds.: J. F. Liebman, A. Greenberg), VCH, Weinheim **1986**, Chapter 3, p. 85; c) R. P. Johnson, *Chem. Rev.* **1989**, *89*, 1111.

[4] a) H. R. Ward, E. Karafiath, *J. Am. Chem. Soc.* **1968**, *90*, 2193; b) H. R. Ward, E. Karafiath, *J. Am. Chem. Soc.* **1969**, *91*, 7475.

[5] T. J. Stierman, R. P. Johnson, *J. Am. Chem. Soc.* **1983**, *105*, 2492.

[6] J. D. Price, R. P. Johnson, *J. Am. Chem. Soc.* **1985**, *107*, 2187.

[7] T. J. Stierman, R. P. Johnson, *J. Am. Chem. Soc.* **1985**, *107*, 3971.

[8] T. J. Stierman, W. C. Shakespeare, R. P. Johnson, *J. Org. Chem.* **1990**, *55*, 1043.

[9] W. C. Shakespeare, R. P. Johnson, *J. Org. Chem.* **1991**, *56*, 6377.

[10] M. W. Klett, R. P. Johnson, *J. Am. Chem. Soc.* **1985**, *107*, 3963.

[11] N. J. Turro, in *Modern Molecular Photochemistry*, Cummings: Menlo Park, CA, **1978**.

[12] a) F. Bernardi, M. Olivucci, M. A. Robb, *Isr. J. Chem.* **1993**, *33*, 265; b) M. Klessinger, *Angew. Chem.* **1995**, *107*, 597; *Angew. Chem. Int. Ed. Engl.* **1995**, *34*, 549; c) F. Bernardi, M. Olivucci, M. A. Robb, *Chem. Soc. Rev.* **1996**, *25*, 321; d) F. Bernardi, M. Olivucci, M. A. Robb, *J. Photochem. Photobiol. A* **1997**, *105*, 365; e) M. Klessinger, *Pure Appl. Chem.* **1997**, *69*, 773.

[13] a) M. Olivucci, I. N. Ragazos, F. Bernardi, M. A. Robb, *J. Am. Chem. Soc.* **1993**, *115*, 3710; b) F. Bernardi, M. Olivucci, I. N. Ragazos, M. A. Robb, *J. Am. Chem. Soc.* **1992**, *114*, 8211.

[14] See the Supporting Information for calculation details.

[15] W. J. Hehre, L. Radom, P. von R. Schleyer, J. A. Pople, *Ab Initio Molecular Orbital Theory*, Wiley, New York, **1986**.

[16] M. J. Bearpark, M. A. Robb, H. B. Schlegel, *Chem. Phys. Lett.* **1994**, *223*, 269.

[17] a) K. Fukui, *J. Phys. Chem.* **1970**, *74*, 4161; b) C. Gonzalez, H. B. Schlegel, *J. Chem. Phys.* **1989**, *90*, 2154.

[18] R. B. Woodward, R. Hoffmann, *Angew. Chem.* **1969**, *81*, 797; *Angew. Chem. Int. Ed. Engl.* **1969**, *8*, 781.

[19] One referee suggested that it is better to explain the shape of the Frank–Condon (FC) region to see in which direction the reaction can take place. The FC point is not a real first-order saddle point. The reason for this is simply because its energy gradient does not go to zero. Even if we draw the picture about the potential-energy surface around the FC point, it is still difficult to recognize in which direction the reaction can take place. Nevertheless, in our study we use figures to represent, for example, the barrier heights, from which one may at least have a quantitative picture about the photochemical reactions. For details, one may see: A. Sanchez-Galvez, P. Hunt, M. A. Robb, M. Olivucci, T. Vreven, H. B. Schlegel, *J. Am. Chem. Soc.* **2000**, *122*, 2911.

[20] The IRC results have highlighted the usefulness of this technique in elucidating reaction mechanisms and have clearly demonstrated what kind of reactions are involved. Those reactions that we have investigated (i.e., paths A-1, A-2, C-1, C-2, C-3, D-1, D-2, D-3, F-1, F-2, F-3, G, H) have been probed in some detail by determining the IRC[17a] with the algorithm proposed by Schlegel[17b].

[21] U. Manthe, H. Koppel, *J. Chem. Phys.* **1990**, *93*, 1658.

[22] a) S. Wilsey, K. N. Houk, *J. Am. Chem. Soc.* **2000**, *122*, 2651; b) S. Wilsey, K. N. Houk, *J. Am. Chem. Soc.* **2002**, *124*, 11182.

[23] a) W. L. Jorgensen, L. Salem, *The Organic Chemist's Book of Orbitals*, Academic Press, New York, **1973**; b) B. Lam, R. P. Johnson, *J. Am. Chem. Soc.* **1983**, *105*, 7479.

[24] However, it was also reported that at least five minor photoproducts (total 13%) were observed but were not isolated in sufficient quantities for complete characterization. For details, see reference [8].

Received: April 27, 2007
Published online: September 18, 2007

